Eur. Phys. J. D **24**, 277–282 (2003)
DOI: 10.1140/epjd/e2003-00189-2

THE EUROPEAN PHYSICAL JOURNAL D

Supersonic cluster beam deposition of nanostructured titania

E. Barborini[1], I.N. Kholmanov[1], A.M. Conti[1], P. Piseri[1], S. Vinati[1], P. Milani[1,a], and C. Ducati[2]

[1] INFM, Dipartimento di Fisica, Università di Milano, Via Celoria 16, 20133 Milano, Italy
[2] Department of Engineering, University of Cambridge, Trumpington Street, Cambridge CB2 IPZ, UK

Received 10 September 2002
Published online 3 July 2003 –

Abstract. Nanostructured titanium dioxide films have been deposited by supersonic cluster beam deposition (CBD). Nanoparticles are produced by a pulsed microplasma cluster source (PMCS) and selected by aerodynamic separation effects. The as-deposited film is a complex mixture where amorphous material coexists, at the nanoscale, with anatase and rutile crystal phases. The nanocrystalline fraction of the film is characterized by crystal size ranging from 100 nm to less than 5 nm. We have characterized the film structure by transmission electron microscopy, Raman spectromicroscopy, X-ray diffraction, and UV-visible spectroscopy showing that correlations exist between cluster size and film properties. In particular if very small clusters are deposited, the film shows a predominant rutile phase whereas larger clusters form films with mainly anatase structure. Our observations suggest that phonon confinement effects are responsible for a significant shift and broadening observed for the Raman peaks. In addition, optical gap tuning is provided by mass selection: large clusters assembling generates a film with 3.22 eV optical gap, while smallest clusters 3.52 eV.

PACS. 77.84.Bw Elements, oxides, nitrides, borides, carbides, chalcogenides, etc. – 81.05.Zx New materials: theory, design, and fabrication – 78.40.-q Absorption and reflection spectra: visible and ultraviolet – 63.22.+m Phonons or vibrational states in low-dimensional structures and nanoscale materials

1 Introduction

Titanium dioxide is one of the most promising semiconductor for applications in microelectronic devices, sensors, photocatalysis, optical coatings, energy production and storage [1–6]. TiO_2 has three polymorphic forms: anatase, rutile, and brookite. Anatase is less stable than rutile and transforms to rutile after annealing at high temperatures [5,7,8].

The physico-chemical properties of TiO_2 are different for different polymorphs and are also influenced by the nanostructure. The control of the crystalline structure at the nanoscale is thus very important for applications. For example anatase and rutile have different electronic and optical properties that can be tailored by varying the size distribution of the particles in nanosized titania [9].

In anatase nanoparticles, down to diameters of roughly 8 nm, broadening and shifting of Raman lines have been observed and attributed to a combination of phonon confinement, deviation from stoichiometry, mechanical stress, and influence of processing conditions [3,10–12]. To clearly distinguish between different effects and to control the final material properties one should be able to tailor the nanostructure of the material and the crystalline structure of the nanoscale building blocks.

Several techniques for the synthesis of nanophase titanium dioxide have been developed: sol-gel processing [13], chemical vapor deposition [14], hydrolysis process [15], colloidal chemistry method [16]. In most cases as-prepared nanostructured titanium dioxide films have an amorphous or amorphous-crystalline polytype structure. In order to obtain more stable phases with well-defined crystalline structure the as-deposited samples usually undergo thermal treatments. In general, material processing by thermal treatment leads to phase transitions, stoichoimetry variations, oxidation and densification which consequently affect the optical, electrical and other physical properties of the material [17–19]. In addition, annealing process significantly changes morphology and texture of the sample [20].

Here we show that nanocrystalline TiO_2 films can be efficiently produced by low energy supersonic cluster beam deposition (CBD). By exploiting the high intensity and mass separation effects typical of supersonic expansions it is possible to deposit TiO_2 films with controlled nanostructure. We show that ultrasmall clusters have a different crystalline structure (anatase or rutile) depending on their dimensions and that it is possible to produce films with controlled nanostructure by selecting the clusters prior to deposition. Analogously, optical band gap of the films can be tuned by selecting precursors with the opportune size. The effects of annealing process on crystal phases and on surface morphology are also presented.

[a] e-mail: pmilani@mi.infn.it

2 Deposition technique

Nanostructured TiO_2 films were grown by depositing clusters produced by a pulsed microplasma cluster source (PMCS), in high vacuum conditions. A detailed description of the PMCS can be found in references [21,22], while its use with titanium in reference [23].

It is known that the supersonic expansion of helium jet exiting PMCS and carrying the titanium clusters causes the radial separation of clusters according to their size: large mass clusters concentrate close to beam axis while smallest ones spread towards the periphery [24]. We have used separation effects to deposit films, with different cluster mass distributions, by intersecting different regions of the beam spot with the substrate. Since clusters maintain, at least partially, their original structure, the films structure is reminiscent of the precursor clusters characteristics.

Another aerodynamic separation technique exploited to separate nanoparticles in a very effective way, according to their mass, is based on an impactor, as in the case of aerosols [25–27]. A surface intercepting a gas flux carrying nano or microparticles induces a sudden turn and decouples the velocity field of the particles from that of the carrier gas. Particles with different masses have different inertia so that a spatial separation takes place and the particles are deposited in different regions of the collecting surface, called impactor. We have demonstrated that the same effects can be used to grow cluster-assembled films with different properties by aerodynamically separating the precursors [23].

Oxidation of titanium clusters constituting the films takes place immediately after exposition to the air, due to the high reactivity of titanium and to the high porosity of the cluster-assembled films. We have verified *a posteriori* the stoichiometry ratio O/Ti $\approx$ 2 by EDAX spectroscopy.

3 Film micro- and nanostructure

Microstructure and surface morphology characterization of the samples were investigated by a scanning electron microscope (SEM) JEOL JSM-IC848 and an atomic force microscope (AFM) Digital Instruments Nanoscope multimode 3A. The grain features observed during SEM measurements are the result of growth dynamics that follow the ballistic aggregation process, typical of low mobility deposition regimes, provided by low energy deposition on cold substrates [28]. Figure 1 reports two SEM images showing the surface of a thin (below 100 nm) and a thick (about 1 μm) film. The observed microscale porosity suggests that a high specific surface area is available.

Transmission electron microscopy (TEM) measurements, performed with a JEOL JEM-4000EX II, 400 KeV, show that cluster-assembled TiO_2 has a structure constituted by nanocrystals and amorphous material. The size of the nanocrystals ranges from 50−100 nm to less than 5 nm, according to the radial spreading of precursor clusters in the supersonic beam: the former sizes are observed

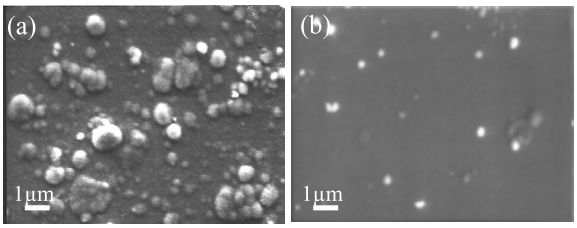

Fig. 1. SEM images showing the surface of films with thickness of about 1 μm (a) and below 100 nm (b). The observed microscale porosity suggests that a high specific surface area is available.

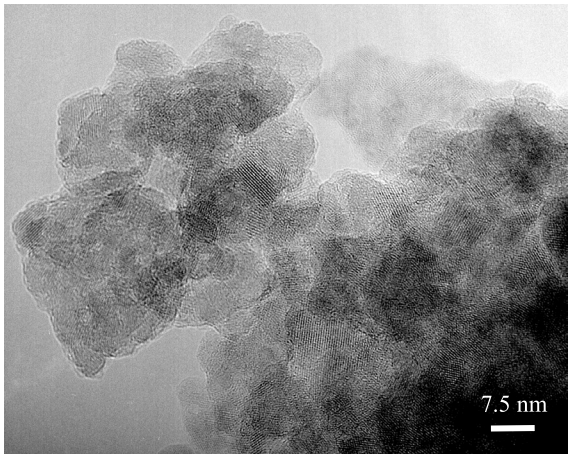

Fig. 2. TEM image showing the nanostructure of the films: grains with size below 10 nm are randomly assembled to constitute a porous structure such as those typical of the ballistic aggregation regime.

in the film grown collecting the clusters close to beam axis, while the latter ones in the film collecting the clusters at the beam periphery. The amorphous fraction is generally visible everywhere, and it becomes the dominant fraction at the beam periphery. In Figure 2 a TEM image is reported showing the nanostructure of the films: grains with size of about 5 nm are randomly assembled to constitute a porous structure such as those typical of the ballistic aggregation regime, as also pointed out by SEM measurements. Nanoparticle lattice spacing and diffraction patterns are consistent with nanocrystalline TiO_2.

4 UV-visible spectroscopy

Optical band gap of cluster-assembled TiO_2 films have been investigated by UV-visible transmittance measurements in the range 190−900 nm. In order to find a correlation of the optical behavior with the size of cluster precursors, measurements have been performed on samples grown by intercepting the cluster beam at different radial positions. Each sample is substantially transparent for wavelength in the visible region, and absorption starts to take place at about $\lambda = 350$ nm. Figure 3a shows an example of transmittance measurements where it is clearly

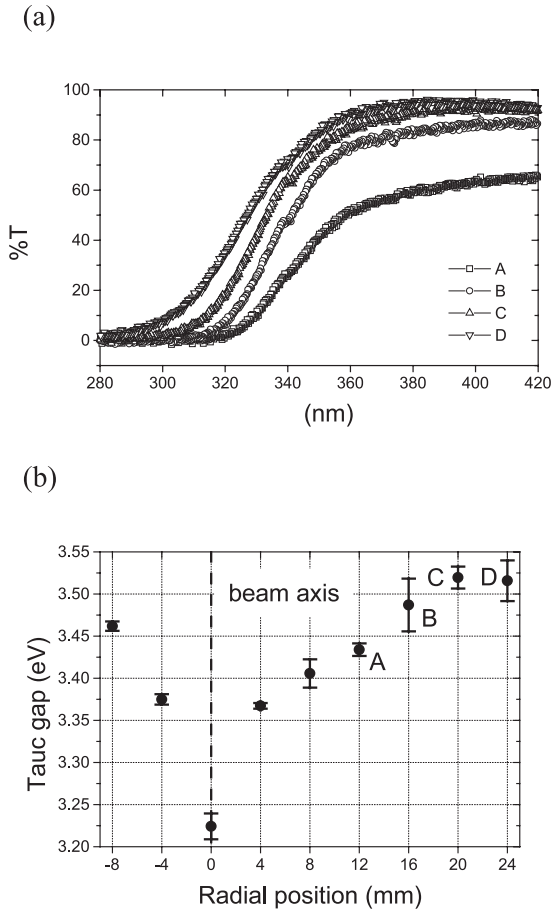

Fig. 3. (a) Example of transmittance measurements. Measure A is taken on a film assembled with large size clusters, while E on a film grown with small size clusters at the periphery of the beam. It is clearly visible the shift of the absorption edge towards higher energy for samples grown with clusters decreasing in size. (b) Correlation between the radial position of the substrate collecting the clusters and the optical gap of the film is shown.

visible the shift of the absorption edge towards higher energy for samples grown with clusters decreasing in size.

The absorption coefficient α, for photons with energy above the threshold of fundamental absorption, follows the $\frac{1}{\omega}(\hbar\omega - E_g)^2$ energy dependence, where $\hbar\omega$ is the photon energy and E_g is the optical energy gap, typical of indirect allowed transitions. Thus the intercept on energy axis in the plot of $\sqrt{\alpha(\omega)\omega}$ *versus* $\hbar\omega$ determines the value of the optical energy gap, the so-called "tauc gap" [29,30]. We calculate E_g of the samples assembled with clusters having different size, and we found values monotonically increasing from 3.22 to 3.52 eV, according to the decreasing of precursors size. In Figure 3b the correlation between the radial position of the substrate collecting the clusters and the optical gap of the film is shown. No dependence has been observed between tauc gap and film thickness.

Transmittance measurements carried out on thickest films (more than 1 μm) also show the interference pattern due to interfaces reflection. The envelope method has been

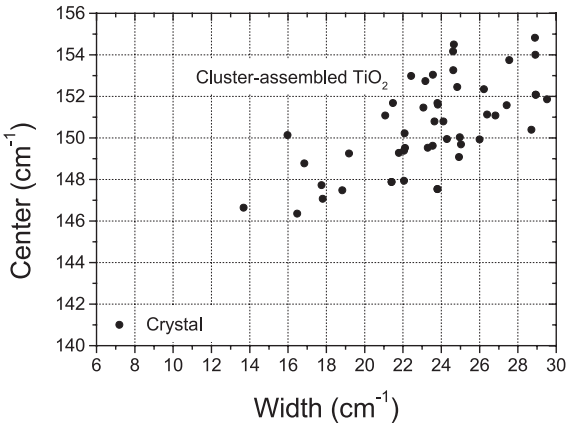

Fig. 4. Scatter plot showing the correlation between center and width of 144 cm^{-1} Raman line, as it results from a fitting procedure based on Lorentzian function, carried out on several samples. In most cases the center shift and the broadening observed in our nanostructured films extend to values larger than those reported in literature, such as $\nu = 155^{-1}$ and $\Gamma = 29^{-1}$.

applied to interference pattern in order to calculate the refraction index [31]. This gave the value of 1.7 for the film assembled with precursor clusters close to beam axis.

5 Raman spectroscopy

Microraman measurements have been carried out by a triple grating Jobin-Yvon T64000 spectrometer, equipped with a Nd:YAG laser (532 nm), and a microscope Olympus BX40. The crystal phase of nanostructured TiO_2 can be characterized by Raman spectroscopy since the two phases, anatase and rutile, have well distinguishable signatures. Anatase has Raman active modes at 144 cm^{-1}, 197 cm^{-1}, 399 cm^{-1}, 513 cm^{-1}, 519 cm^{-1}, 639 cm^{-1}, while rutile at 143 cm^{-1}, 447 cm^{-1}, 612 cm^{-1}, 826 cm^{-1} [13].

Moreover, various studies are reported in literature showing that a correlation exists between the center and the width of the 144 cm^{-1} anatase mode, and between them and the size of crystals in the material, caused by relaxation of $q = 0$ selection rule [10,32]. Due to the fact that in our samples both phases coexist (with variable ratio, as it will be explained below) and separation only involves the cluster sizes, the analysis of the 144 cm^{-1} Raman line furnishes information, alternative to TEM, on the size of nanocrystals. A fitting procedure of 144 cm^{-1} Raman line based on Lorentzian function has been carried out giving very good interpolation results. The center and the width of the peak coming from the fit on several samples are correlated, as shown in Figure 4, and disperse themselves according to the curve known from literature [9]. In most cases the center shifts and the broadening observed in our nanostructured films extend to values larger than those reported in literature, such as $\nu = 155$ cm^{-1} and $\Gamma = 29$ cm^{-1}, related to crystal size well below 10 nm.

As explained above, the internal surface of PMCS nozzle acts as an impactor causing the separation of clusters

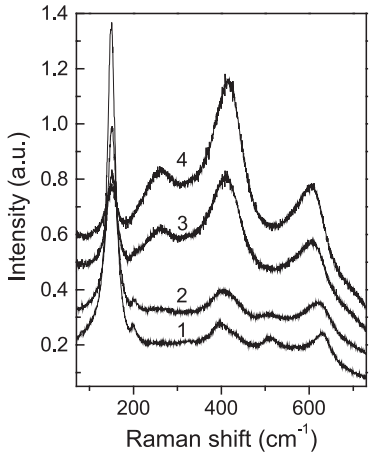

Fig. 5. Raman spectra obtained by sampling the impactor at different positions. Bottom spectrum (1) refers to the region where largest clusters have been aerodynamically selected and deposited, while top spectrum (4) refers to region of smallest ones. The film assembled with large clusters has a predominant anatase structure, as indicated by the peaks at 150, 204, 399, 513, 635 cm^{-1}, that correspond to those of bulk anatase, with some shifting and broadening. Following the progressive decreasing of TiO_2 nanocrystallite size, the Raman spectra evolve towards that of rutile phase (4).

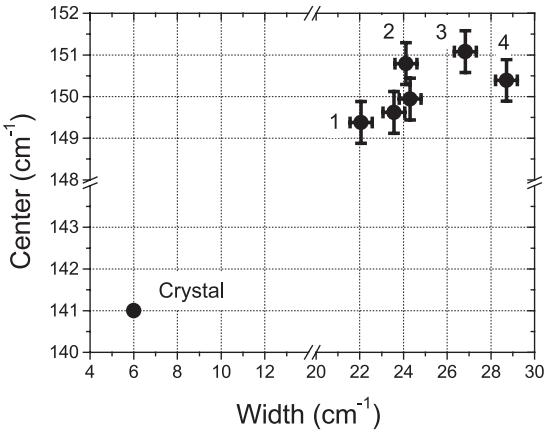

Fig. 6. Correlation between the width and the center of the 144 cm^{-1} peak of the spectra in Figure 5. The peak behavior is a clear indication of the decrease of the nanocrystallite dimensions moving from the anatase region to the rutile one.

according to their mass [23]. Raman spectra obtained by sampling the impactor at different positions are reported in Figure 5. Bottom spectrum refers to the region where largest clusters have been aerodynamically selected and deposited, while top spectrum refers to region of smallest ones. The presence of a predominant anatase nanocrystalline structure is thus indicated in the film assembled with large clusters. The peaks at 150, 204, 399, 513, 635 cm^{-1} correspond to those of bulk anatase, with some shifting and broadening. In particular the 144 cm^{-1} peak is blue shifted at 150 cm^{-1}, while the 635 cm^{-1} peak is red-shifted. Moving towards top spectrum, the bands at 150, 204, 513 cm^{-1} decrease in intensity, while the peaks at 399 and 635 cm^{-1} broaden and show a blue- and red-shift respectively. Following the progressive decreasing of TiO_2 nanocrystallite size, the Raman spectra evolve towards that of rutile phase (top spectrum). Rutile peaks, as reported in [32], appear, together with the strong combination band at 235 cm^{-1}.

Moving from the anatase-like spectrum (bottom) to the rutile-like spectrum (top) we observe that the 144 cm^{-1} peak broadens and it is blue-shifted, consistently with the decreasing in crystallite size. As done in Figure 4, Figure 6 shows the correlation between the width and the center of the anatase peak of various spectra acquired from regions containing different cluster sizes. The peak behavior is a clear indication of the decrease of the nanocrystallite dimensions going from the anatase region to the rutile one. Our measurements suggest that only confinement effects related to cluster dimensions are responsible for the observed Raman spectra modifications.

6 Annealing

The effects of thermal treatments on the structure and morphology have been also studied. This investigation involved the films assembled with small-size clusters contained into the beam periphery. Annealing were performed inside a cylindrical furnace by holding the samples on a cylindrical quartz tube with open ends, under ambient atmosphere. The samples were kept at temperatures of 200, 400, 600, and 800 °C with duration of 4 hours at each annealing step. Crystalline phase evolution was studied by X-ray Diffraction (XRD) spectrum analysis using a Philips PW 1830 X-ray diffractometer with Cu Kα-radiation, while morphology with AFM.

XRD spectra of the as-deposited and annealed samples are shown in Figure 7. As pointed out by TEM measurements, as-deposited films are composed of an amorphous structure, generating a broad bump centered at about $2\theta = 26°$, together with mixture of anatase and rutile crystalline phases. Nevertheless, due to nanosize of crystallites the XRD signatures of these phases melt into a unique unresolved structure, at about $2\theta = 55°$, accounting for both.

The spectrum of the specimen after the thermal treatment at a temperature of 200 °C is very similar to that of the as-deposited sample with little increasing of the peak intensities. Dramatically changes of the crystalline structure are observed after annealing the sample at 400 °C. The low intensity amorphous peak is replaced by an intense and sharp peak at about $2\theta = 25.4°$ which is attributed to anatase phase. This changing shows that the amorphous-anatase phase transition takes place below 400 °C. After annealing at 600 °C the peaks corresponding to anatase phase become more intense and sharper, exhibiting that at this temperature the nanoparticles are crystallized mainly in anatase phase. Further annealing at 800 °C leads to the appearance of intense peaks related to rutile phase and causes the decreasing of anatase peak intensities.

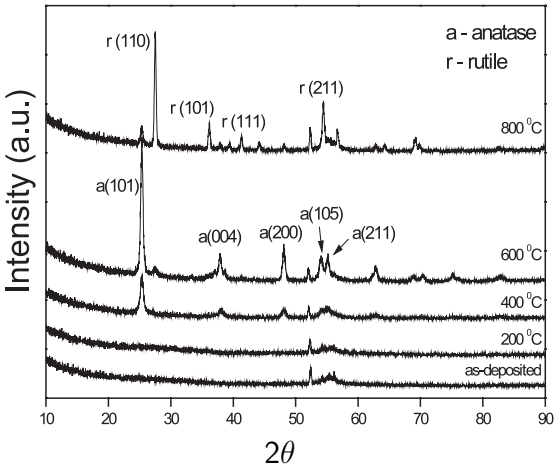

Fig. 7. XRD spectra of the as-deposited and annealed samples. As-deposited films (bottom) are composed of an amorphous structure, generating a broad bump centered at about $2\theta = 26°$, together with mixture of anatase and rutile nanocrystalline phases, producing the unresolved structure, at about $2\theta = 55°$, accounting for both. Changes of the crystalline structure are observed after 400 °C annealing. The low intensity amorphous peak is replaced by an intense and sharp peak at about $2\theta = 25.4°$ which is attributed to anatase phase. This change shows that the amorphous-anatase phase transition takes place below 400 °C. After annealing at 600 °C the peaks corresponding to anatase phase become more intense and sharper, exhibiting that at this temperature the nanoparticles are crystallized mainly in anatase phase. Further annealing at 800 °C leads to the appearance of intense peaks related to rutile phase and causes the decreasing of anatase peak intensities, as known in literature.

The XRD analysis reveals that the surface of the deposited film is stoichiometric TiO_2, and that the phase transitions amorphous-anatase and anatase-rutile take place below 400 °C and at 800 °C, respectively. Similar amorphous-anatase and anatase-rutile phase transition have been observed in TiO_2 thin films produced by other methods [33,34].

Morphology changes after annealing were studied AFM. The as-deposited films consist of fine-grained spheroid nanoparticles with mean size of about 10 nm. Surface features are consistent with the ballistic aggregation growth process. After 800 °C annealing, the film became more dense and exhibits an oriented growth direction with columnar structure. The original spheroid shape of surface features turns into polyhedral, accounting for the crystallization of nanostructured TiO_2 into a polycrystalline material. These observations are summarized in Figure 8.

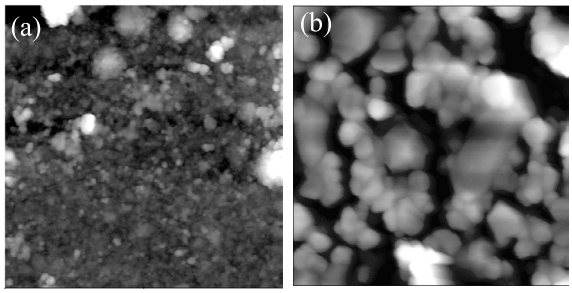

Fig. 8. AFM pictures showing the morphology changes after annealing. The as-deposited films (a) consist of fine-grained spheroid nanoparticles with mean size of about 10 nm. Surface features are consistent with the ballistic aggregation growth process. After 800 °C annealing (b), the film became more dense, and the original spheroid shape of surface features turns into polyhedral, accounting for the crystallization of nanostructured TiO_2 into a polycrystalline material. The side of the images is 2 μm.

7 Conclusions

In conclusion, we have produced nanocrystalline TiO_2 films with controlled structure by depositing, at room temperature, clusters selected from gas phase according to their size. Beside an almost uniformly dispersed amorphous phase, in the film nanocrystals have sizes in the range from 50−100 nm to less than 5 nm. Films with predominant anatase or rutile structure can be grown by aerodynamically selecting clusters with different diameters. The optical gap of the samples also has been demonstrated to depend on cluster precursor size in such a way that it monotonically increases from 3.22 to 3.52 eV, according to the decreasing of precursors size. These results disclose the possibility to tailor the physico-chemical properties of nanostructured TiO_2 films by selecting the correct precursor size before deposition. Moreover, the low temperature involved in the deposition process is interesting for the production of films on thermolabile substrates and filters to be used for photocatalysis, antibacterial coatings and water purification.

The effect of thermal treatments on films assembled with small clusters has been studied after annealing at various temperatures, and the phase transitions amorphous-anatase and anatase-rutile have been observed below 400 °C and after 800 °C, respectively. Several authors studied the role of crystal size on phase evolution during annealing procedure [35,36]. This matter is currently investigated in the case of cluster assembled TiO_2.

Morphology studies of the samples by AFM show that the sample surface has large porosity and consists of fine-grained spheroid nanostructures with a mean size of about 10 nm. After annealing spheroid shaped surface features evolve to polyhedral shapes indicating crystallization of the samples.

We are grateful to Silvia Maffi for XRD measurements. We thanks S. Iannotta and P. Siciliano for useful discussions. This work has been supported by Provincia Autonoma di Trento under Project RASO.

References

1. M. Grätzel, in *Semiconductor Nanoclusters – Physical, Chemical and Catalytic Aspects*, edited by P.V. Kamat, D. Meisel (Elsevier, Amsterdam, 1997), p. 353

2. C. Garzella, E. Comini, E. Tempesti, C. Frigeri, G. Sbervegliere, Sensors Actuat. B **68**, 189 (2000)
3. M. Grätzel, Nature **414**, 338 (2001)
4. Z. Guan, X. Zhang, Y. Ma, Y. Cao, J. Yao, J. Mater. Res. **16**, 907 (2001)
5. J.C. Parker, R.W. Siegel, Appl. Phys. Lett. **57**, 943 (1990); J. Mater Res. **5**, 1246 (1990)
6. M. Anpo, Pure Appl. Chem. **72**, 1265 (2000)
7. S.D. Mo, W.Y. Ching, Phys. Rev. B **51**, 13023 (1995)
8. M. Lazzeri, A. Vittadini, A. Selloni, Phys. Rev. B **63**, 155409-1 (2001)
9. R.J. Gonzalez, R. Zallen, *Amorphous Insulators and Semiconductors*, NATO-ASI, edited by M.F. Thorpe, M.I. Mitkova (Kluwer, Dordrecht, 1997), p. 395
10. D. Bersani, P.P. Lottici, X.Z. Ding, Appl. Phys. Lett. **72**, 73 (1998)
11. A.G. Gaynor, R.J. Gonzalez, R.M. Davis, R. Zallen, J. Mater. Res. **12**, 1755 (1997)
12. W.F. Zhang, Y.L. Ye, M.S. Zhang, Z. Yin, Q. Chen, J. Phys. D: Appl. Phys. **33**, 912 (2000)
13. P.P. Lottici, D. Bersani, M. Braghini, A. Montenero, J. Mater. Sci. **28**, 177 (1993)
14. A. Goossens, E.-L. Maloney, J. Schoonman, Chem. Vap. Deposit. **4**, 109 (1998)
15. W.F. Zhang, M.S. Zhang, Z. Yin, Phys. Stat. Sol. (a) **179**, 319 (2000)
16. W. Ma, Z. Lu, M. Zhang, Appl. Phys. A **66**, 621 (1998)
17. J.D. DeLoach, G. Scarel, C.R. Aita, J. Appl. Phys. **85**, 2377 (1999)
18. M.H. Suhail, G. Mohan Rao, S. Mohan, J. Appl. Phys. **71**, 1421 (1992)
19. K. Fukushima, I. Yamada, J. Appl. Phys. **65**, 619 (1989)
20. L.M. Williams, D.W. Hess, J. Vac. Sci. Technol. A **1**, 1810 (1983)
21. E. Barborini, P. Piseri, P. Milani, J. Phys. D: Appl. Phys. **32**, L105 (1999)
22. P. Piseri, A. Podesta', E. Barborini, P. Milani, Rev. Sci. Instrum. **72**, 2261 (2001)
23. E. Barborini, I.N. Kholmanov, P. Piseri, C. Ducati, C.E. Bottani, P. Milani, Appl. Phys. Lett. **81**, 3052 (2002)
24. E. Barborini, P. Piseri, A. Li Bassi, A.C. Ferrari, C.E. Bottani, P. Milani, Chem. Phys. Lett. **300**, 633 (1999)
25. J. Fernandez de la Mora, N. Rao, P.H. McMurry, J. Aerosol Sci. **21**, 889 (1990)
26. H. Vahedi Tafreshi, P. Piseri, S. Vinati, E. Barborini, G. Benedek, P. Milani, Aerosol Sci. Technol. **36**, 593 (2002)
27. W.T. Nichols, J.W. Keto, D.E. Henneke, J.R. Brock, G. Malyavanatham, M.F. Becker, H.D. Glicksman, Appl. Phys. Lett. **78**, 1128 (2001)
28. L. Bardotti, B. Prevel, P. Melinon A. Perez, Q. Hou, M. Hou, Phys. Rev. B **62**, 2835 (2000)
29. J. Tauc, *Amorphous and liquid semiconductors* (Plenum Press, London, 1974), p. 159
30. P. Madhu Kumar, S. Badrinarayanan, Murali Sastry, Thin Solid Films **358**, 122 (2000)
31. Han-Yong Joo, Hyeong Joon Kim, Sang June Kim, Sang Youl Kim, J. Vac. Sci. Technol. A **17**, 862 (1999)
32. Z. Iqbal, S. Veprek, J. Phys. C: Solid State Phys. **15**, 377 (1982)
33. M.D. Wiggins, M.C. Nelson, C.R. Aita, J. Vac. Sci. Technol. A **14**, 772 (1996)
34. J.A. Eastman, J. Appl. Phys. **75**, 770 (1994)
35. S.C. Liao, W.E. Mayo, K.D. Pae, Acta Mater. **45**, 4027 (1997)
36. H. Zhang, M. Finnegan, J.F. Banfiels, Nano Lett. **1**, 81 (2001)